applied sciences

MDPI

Article

Sub-Meter Spatial Resolution Phase-Sensitive Optical Time-Domain Reflectometry System Using Double Interferometers

Shengwen Feng [1,2], Tuanwei Xu [1,2,*], Jianfen Huang [1,2], Yang Yang [3], Lilong Ma [1,2] and Fang Li [1,2]

1 Key Laboratories of Transducer Technology, Institute of Semiconductors, Chinese Academy of Sciences, Beijing 100083, China; swfeng@semi.ac.cn (S.F.); jfhuang@semi.ac.cn (J.H.); malilong@semi.ac.cn (L.M.); lifang@semi.ac.cn (F.L.)

2 College of Materials Science and Opto-Electronic Technology, University of Chinese Academy of Sciences, Beijing 100089, China

3 School of Physics and Microelectronics, Hunan University, Changsha 410082, China; y_yang@hnu.edu.cn

* Correspondence: xutuanwei@semi.ac.cn; Tel.: +86-010-8230-5480

Received: 13 August 2018; Accepted: 5 October 2018; Published: 12 October 2018

Abstract: An improved phase-sensitive optical time-domain reflectometry (φ-OTDR) system with sub-meter spatial resolution is demonstrated. Two Michelson interferometers (MIs) with different path length differences are used in the proposed system. One is 10 m, the other is 9.2 m. Two Rayleigh backscattering phase traces with different spatial resolution are obtained by a phase generated carrier (PGC) algorithm at adjacent times. After using differencing and adaptive 2-D bilateral filtering algorithms, a 0.8-m spatial resolution over 2 km is achieved. Experimental results indicate that the system shows an extraordinary linearity as high as 99.94% with amplitude-modulation and acquires a detection frequency from 5 to 500 Hz.

Keywords: backscattering; optical sensing and sensors; fiber optics sensors

1. Introduction

Phase-sensitive optical time-domain reflectometry technology is widely used in distributed optical fiber sensing systems for intrusion detection, pipeline condition monitoring, oil and gas exploration, etc. [1–3]. In early research, much effort was put towards detecting the interfering amplitude resulting from the external vibration signal. However, these intensity demodulation methods cannot restore the full scale external vibration signal information for the nonlinearity between the changed interfering amplitude and the demodulated magnitude of vibration-induced perturbation. To overcome this obstacle, so-called fiber-optic distributed acoustic sensing (DAS) has been proposed, making DAS a research hotspot in recent years [3–21].

With external vibration reaching the sensing fiber, the local refractive index and length will modulated, which leads to the relative linear phase change. Unlike intensity demodulation methods, DAS technology focuses on detecting the phase that directly represents the external vibration signal. Up to now, DAS systems contain two different demodulation schemes; direct detection [6–10] and coherent detection [11–16]. The system demonstrated in Reference [6] has a spatial resolution of 2 m with a frequency range of 500–5000 Hz. The system in Reference [7] is based on PGC demodulation, which has a maximum sensing length of 10 km and a spatial resolution of 6 m. Reference [8] introduces a distributed temperature and strain system by using linearly chirped pulses, which can achieve a 1 mK/4 nε resolution with a spatial resolution of 10 m over 1 km. Reference [15] reports a system based on I/Q demodulation and homodyne detection, which has a sensing range of 12.56 km and a spatial resolution of

10 m. These above systems' spatial resolution are in the range of tens of meters or meters, which cannot satisfy the high spatial resolution demand in some special applications, for example, the crack detection. To further improve the spatial resolution, an improved optical arrangement and a new signal processing procedure are used in the system in Reference [9], which can detect dynamic perturbations in 5 km with a spatial length of 50 cm. Three independent photodiodes, operated in synchronism, are required in this scheme. The spatial resolution of this scheme is still limited by the path difference of imbalanced Mach–Zehnder interferometer (MZI). With an optical frequency swept pulse, the system in Reference [16] achieved a sensing distance of 19.8 km and a spatial resolution of 30 cm and a signal-to-noise ratio (SNR) of 10 dB for vibration sensing. The spatial resolution of the optical frequency swept pulse optical time-domain reflectometry (φ-OTDR) is determined by the frequency sweeping range. The authors use a moving differential technique to determine the phase change, which can only be used to determine the change in amplitude of the backscattering and has a low SNR. In addition, this scheme requires a relatively high bandwidth photodetector and a high sampling rate data acquisition card, thus introducing difficulty in real-time measurement.

In this article, we introduce an alternative to improve the spatial resolution of a φ-OTDR system by using double interferometers, which breaks through the limits set by the path difference of Michelson interferometers (MIs). Two MIs with different path length differences are used in the system. One is 10 m, the other is 9.2 m. Trough precise time control and PGC algorithm, the phase of Rayleigh scattering (RS) light along the sensing fiber can be obtained in an adjacent time. After using a heterodyne and 2-D bilateral filtering algorithm, a 0.8 m spatial resolution over 1.9 km is demonstrated in the experiment.

2. Proposed Sub-Meter Spatial Resolution φ-OTDR: Theoretical Model

The working principle of the proposed φ-OTDR system is to detect the phase change induced by the coherent RS caused by multiple scattering centers within the injected pulse duration. A narrow-linewidth laser is modulated by an acousto-optic modulator (AOM) to produce a short optical pulse. The short optical pulse is launched into the sensing fiber and the returned RS light is sent to the imbalanced MIs. Then the photodetector (PD) collects the interfering RS light after MI; the interference light from a certain position, L, with a time delay, which is caused by the optical path difference, L_{MI}, in MI, the interference light intensity from the position L can be given as [7]:

$$E(t) = E_L(t) + E_{L-L_{MI}/2}(t) = A + B\exp[j\beta L_{MI} + \Delta\varphi_L(t)] \quad (1)$$

where $\Delta\varphi(t) = \varphi_{L-L_{MI}/2}(t) - \varphi_L(t)$ is the phase change carrying the sensing information related to external disturbance, and A and B are the simplified coefficients. The intensity of the interference light from MI is given by [7]:

$$I(t) = |E(t)|^2 = I_D + I_c\cos[\beta L_{MI} + \Delta\varphi] \quad (2)$$

where $I_D = A^2 + B^2$ and $I_c = 2AB$. After using a PGC algorithm and arctangent operation, phase information can be recovered by arctangent operation as follows [7]:

$$\varphi(t) = \arctan[I(t)/Q(t)] \quad (3)$$

where $I(t)$ and $Q(t)$ are the in-phase and quadrature components, respectively.

The experimental system setup is illustrated in Figure 1. An arbitrary function generator (AFG) generated two different periodic signals; a narrow pulse signal (red line, 1) and a sinusoidal signal (purple line, 2). The pulse signal was used to drive an acousto-optic modulator (AOM) and control the optical switch on-off. The sinusoidal signal was intended for modulating a piezoelectric ceramic transducer and applied for phase-generated carrier demodulation. A continuous light from a narrow line-width laser with the wavelength of 1550.15 nm and linewidth of 3 kHz was modulated by an AOM (insertion loss 5 dB; extinction ratio 50 dB) as optical pulse, of which the duration time and repetition

rate were 50 ns and f_r = 8 kHz. The optical pulse was amplified by an erbium-doped fiber amplifier (EDFA). An optical isolator was used to prevent any backward amplified spontaneous emission (ASE) generated in the EDFA from causing instabilities or damage to the laser. A fiber Bragg grating (FBG) with a center wavelength of 1550.35 nm, 3 dB bandwidth of 0.25 nm and reflectivity of 99.6% was utilized for eliminating forward ASE from the EDFA. The filtered light was launched into the sensing fiber through a circulator. After that, the backscattering light was, in turn, injected into the two unbalanced MIs (MI1 and MI2), comprised of a coupler and two Faraday rotation mirrors (FRMs) controlled by the optical switch that is synchronized with the pulse signal. The two MIs were almost the same, except that the path length difference of MI1 and MI2 were L_{MI1} = 10 m and L_{MI2} = 9.2 m, respectively. A sinusoidal electrical signal with oscillation frequency of f = 2 kHz was applied to the piezoelectric transducer (PZT) placed at one arm of the MIs for the PGC algorithm. Interfering signal was collected by a high sensitive balance photodetector (BPD, bandwidth 200 MHz, transimpedance gain 60 kV/A). The output of BPD and the sinusoidal signal were transferred to a data acquisition and signal processing unit to retrieve the phase information. An isolator was employed at the end of the sensing fiber to remove unwanted end reflection.

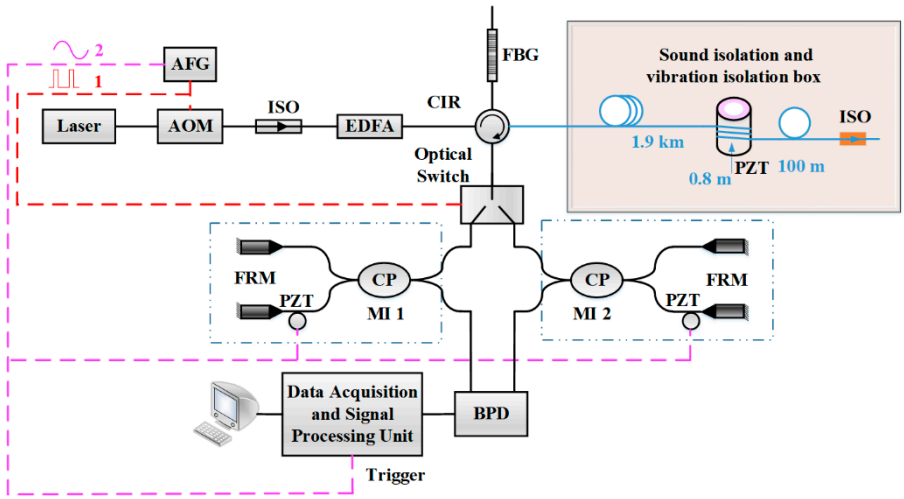

Figure 1. Experimental setup.

The output of BDP for the two MIs-related signals can be expressed as:

$$\begin{aligned} I_1(t) &= I_{D1} + I_{c1}\cos[\beta L_{MI1} + \Delta\varphi_1] \\ I_2(t) &= -I_{D2} - I_{c2}\cos[\beta L_{MI2} + \Delta\varphi_2] \end{aligned} \tag{4}$$

The above signals are in turns obtained in a short time ($T = 1/f_r$, f_r = 8 kHz). The spatial resolution of the proposed system is defined as the gauge length [6,7], that is L_{MI}. As a result, a series of trains of backscattered traces were obtained (Figure 2). In Figure 2, the blue line represents the MI1-related RS intensity trace, and the red line is associated with MI2. The interval between the two traces is $T = 1/f_r$, which is the optical switch's on-off time. The acquired RS traces were sent to the data acquisition card (DAQ) and signal processing unit. Then through the PGC algorithm, the phase information with a different spatial resolution along the whole sensing fiber was achieved.

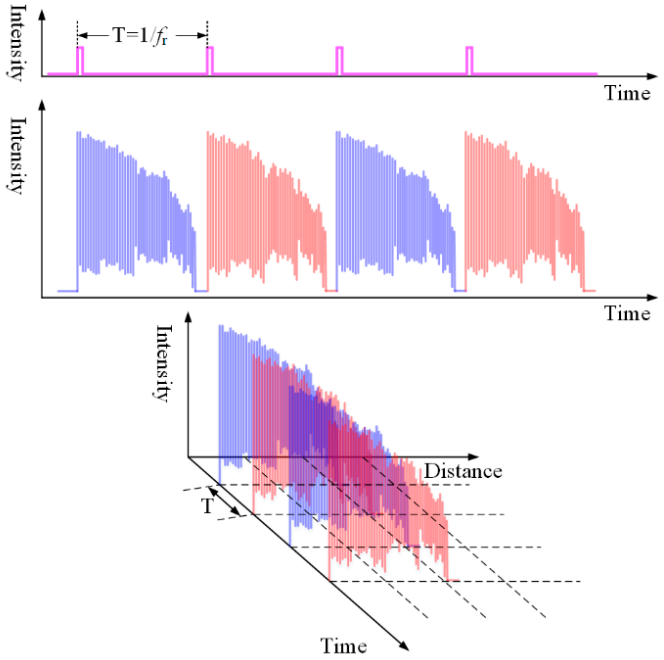

Figure 2. Diagram of Raleigh backscattered traces for MI1 (Blue) and MI2 (Red).

Figure 3 is a schematic of the differencing approach for enhanced spatial resolution in the system. The external disturbance lead to a change in the effective refractive index and fiber length and resulted in the phase changing. A series of phase traces with a spatial resolution of L_{MI1} and L_{MI2} were acquired for MI1 and MI2, respectively. Then, through the differencing approach, i.e.,

$$\phi = \Delta\varphi_1 - \Delta\varphi_2 \tag{5}$$

an improved spatial resolution of phase information was achieved.

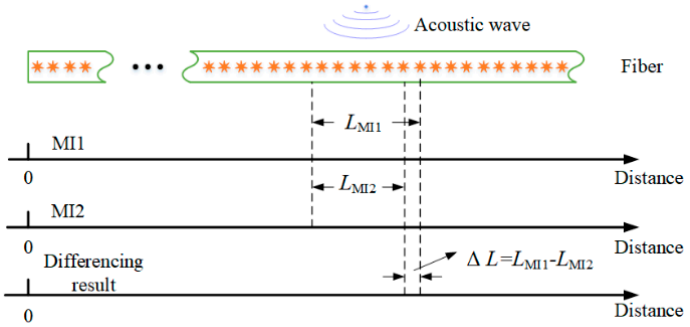

Figure 3. A schematic of the heterodyne approach for enhanced spatial resolution in the system.

3. Vibration Measurement

As presented in Figure 1, bare fiber with a length of 0.8 m was coiled over a cylindrical PZT at a position of ~1.9 km. A sinusoidal electrical signal with a peak-to-peak voltage of 0.8 V and a frequency of 20 Hz from a signal generator was applied on PZT. The left side of Figure 4a,c,e is the 3D plot of spatial-temporal domain demodulated signals after using an adaptive 2-D bilateral filtering algorithm, which is used to remove the undesired noise effectively [22]. The unit of channel was 0.4 m, called as spatial sampling resolution is determined by the DAQ card sampling rate of 250 MS/s. The unit of time was 0.5 ms, which is the reciprocal of the oscillation frequency of the sinusoidal PGC signal. The right side of Figure 4b,d,f is the normalized strain distribution envelope from the 1st to the

180th channel around 1.9 km along the fiber. The strain distribution envelope was obtained through the superimposition of each trace over a period of time after amplitude normalization.

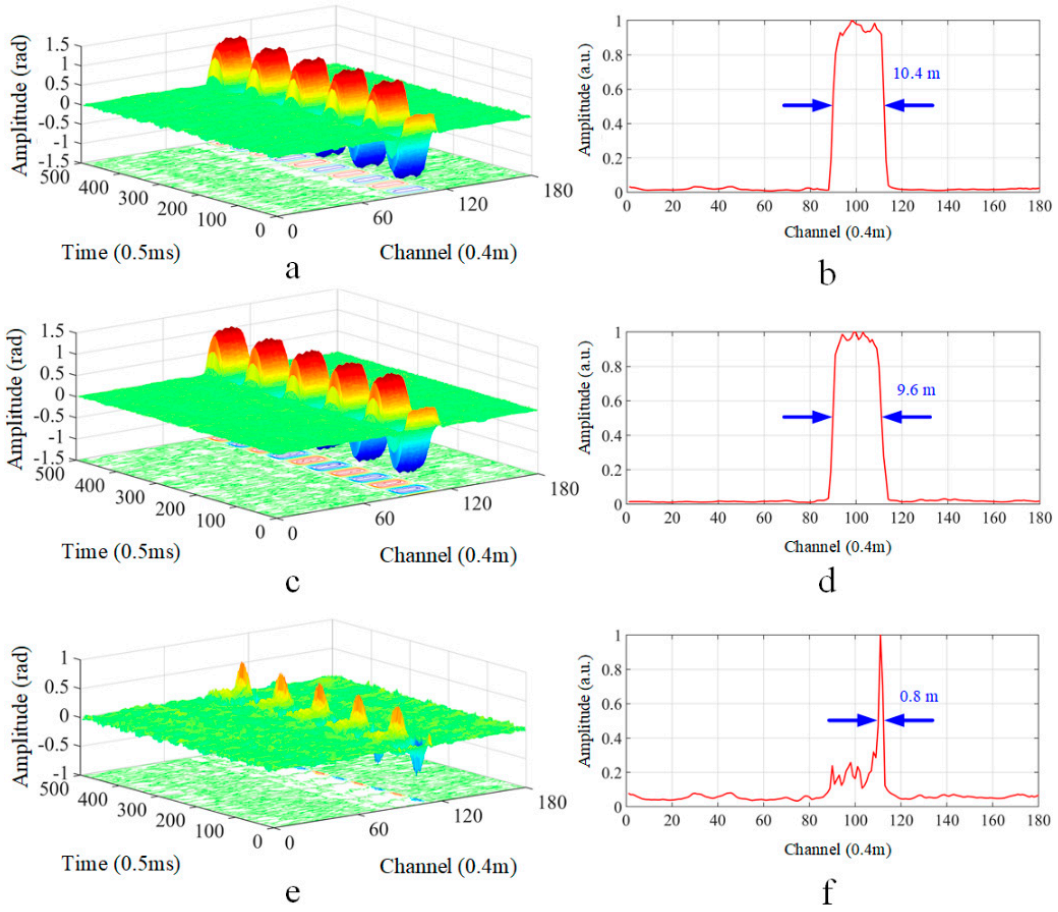

Figure 4. 3D plot of spatial-temporal domain demodulated signals (**a**,**c**,**e**) and strain distribution envelope (**b**,**d**,**f**) from 0 to 180 m positions around 1.9 km along the fiber. MI1: (**a**,**b**); MI2: (**c**,**d**); Heterodyne results: (**e**,**f**).

Figure 4a,b are demodulated results related to MI1, Figure 4c,d are relevant to MI2 and Figure 4e,f are the results after the differencing operation. Here, the full width at half maximum (FWHM) of the strain distribution envelope is defined to the ultimate spatial resolution. According to Figure 4b,d, the spatial resolution of MI1-relevant and MI2-relevant were 10.2 m and 9.4 m, respectively. After the differencing approach, an improved spatial resolution of 0.8 m was obtained for the DAS system (shown in Figure 4f).

Figure 5 is the demodulated results of the 111th channel in the time and frequency domains. The red line and green line are related to MI1 and MI2, and the blue dot dash line is the differencing result. It seems that the time and frequency domain information of the MI2-relevant trace and the differencing result are almost the same. This is just a coincidence, because, at this test, the magnitude of the demodulation signal of the MI1-relevant trace happens to be twice as much as that of MI2's. In addition, it should be pointed that the magnitude of the differencing result will meet an inevitable loss, which is originated from the difference algorithm. Particularly, it should be noted that the noise floor of the combined results seems slightly higher in the region where the two different spatial resolution traces were subtracted. The new noise floor comes from the differencing operation and the randomness of RS amplitude along the fiber. Because the two MIs are not perfectly identical, the demodulated phase information of the two MIs is not perfectly decoupled. Furthermore, the normalization operation contributes a lot to the increase of the noise floor.

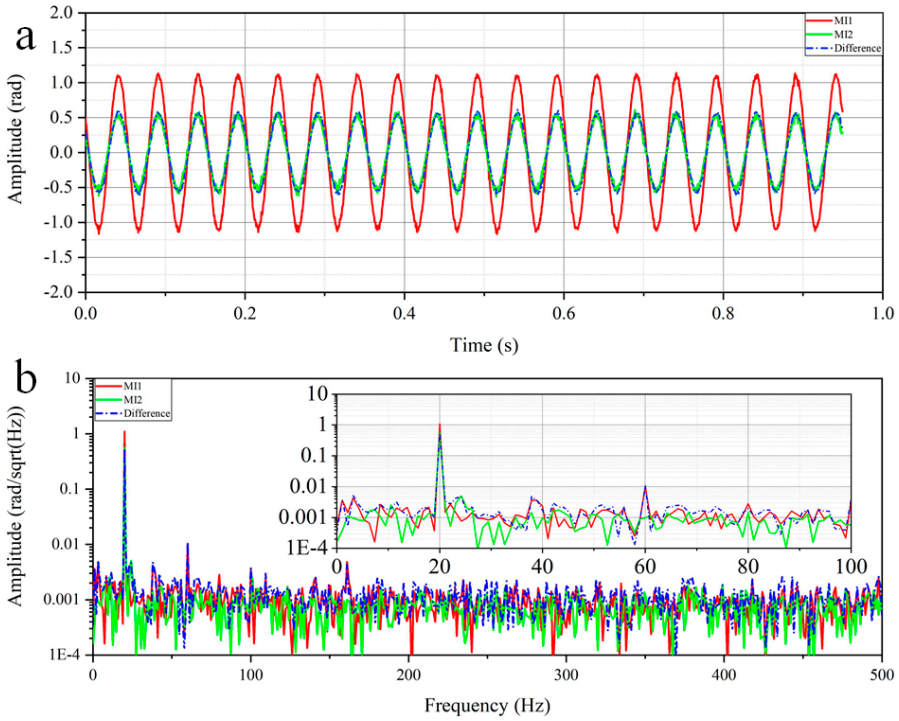

Figure 5. (**a**) The measurement result of a 20 Hz vibration and (**b**) the corresponding spectrum of the 111th trace.

To gain a better understanding of the performance of the DAS system, amplitude-modulation (AM) and frequency-swept (FS) modulation were conducted. Without loss of generality, in the following test, only the differencing area result was investigated.

In the AM test, a 100 Hz sinusoidal signal with the voltage varying from 10 mVpp to 1.6 Vpp is applied on the PZT to inspect the strain response of the DAS system. In Figure 6, the square black spots represent the demodulated results of the system, and the red line is the fitting curve, which declares that the measurement data fit excellently with a linearity of 99.94%.

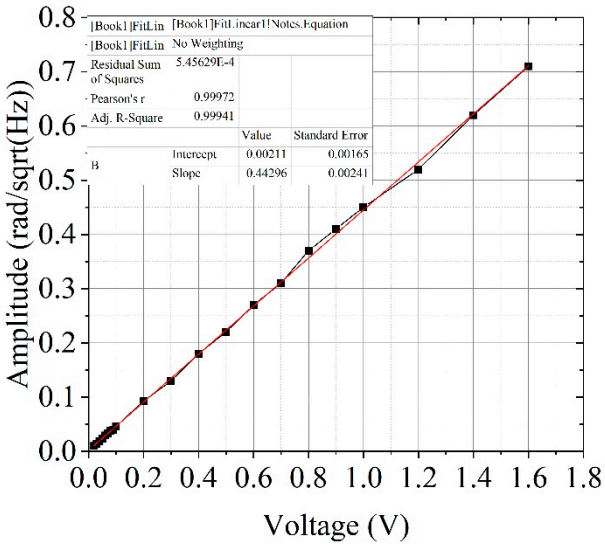

Figure 6. The demodulated amplitude versus voltage for 100 Hz frequency sinusoidal wave.

An FS test was carried out to study the frequency response of the DAS system. A linear FS sine waveform from 5 to 500 Hz, a 4 s sweep time and 1 Vpp amplitude, were applied to the PZT. A short

time Fourier spectrogram was performed to describe the time-frequency information, as shown in Figure 7, which visually displays the linearity of sweep frequency and relative flat frequency response.

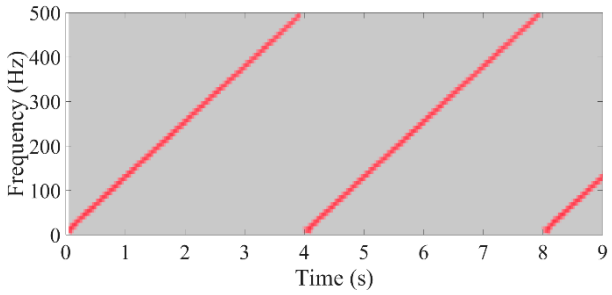

Figure 7. The short time Fourier spectrogram of the demodulated result of the FS signal.

4. Conclusions

In this paper, an improved sub-meter spatial-resolution φ-OTDR system, using a double MIs differencing algorithm, is proposed. The strain response and frequency response are investigated, which demonstrate a linear strain response (as high as 99.94%) and a flat frequency response from 5 to 500 Hz. The utmost limit of the spatial resolution of the proposed system was determined by the spatial sampling resolution, which was dependent on the sampling rate of the data acquisition card. In addition, the rise-time/fall time of the acousto-optic modulator and the photodetector must be taken into consideration. For a 0.1 m spatial resolution, a 1 GS/s sampling rate and different path length difference of 0.1 m, together with less rise-time/fall time of the acousto-optic modulator and photodetector, are needed, which will bring about an enormous challenge for real-time demodulation.

Author Contributions: S.F. and T.X. wrote the paper. All the authors reviewed and critiqued the manuscript.

Funding: This research was funded by [National Natural Science Foundation of China] grant number [61775210 and 61875184] and [National Key Research and Development Program of China] grant number [2017YFB0405500].

Acknowledgments: The authors wish to acknowledge the financial support of National Natural Science Foundation of China and National Key Research and Development Program of China.

Conflicts of Interest: The authors declare no conflict of interest.

References

1. Juarez, J.C.; Maier, E.W.; Kyoo Nam, C.; Taylor, H.F. Distributed fiber-optic intrusion sensor system. *J. Light. Technol.* **2005**, *23*, 2081–2087. [CrossRef]
2. Tanimola, F.; Hill, D. Distributed fibre optic sensors for pipeline protection. *J. Nat. Gas Sci. Eng.* **2009**, *1*, 134–143. [CrossRef]
3. Parker, T.; Shatalin, S.; Farhadiroushan, M. Distributed Acoustic Sensing—A new toolfor seismic applications. *First Break* **2014**, *32*, 61–69. [CrossRef]
4. Qin, Z.; Chen, L.; Bao, X. Continuous wavelet transform for non-stationary vibration detection with phase-OTDR. *Opt. Express* **2012**, *20*, 20459–20465. [CrossRef] [PubMed]
5. Daley, T.M.; Freifeld, B.M.; Ajo-Franklin, J.; Dou, S.; Pevzner, R.; Shulakova, V.; Kashikar, S.; Miller, D.E.; Goetz, J.; Henninges, J.; et al. Field testing of fiber-optic distributed acoustic sensing (DAS) for subsurface seismic monitoring. *Lead. Edge* **2013**, *32*, 699–706. [CrossRef]
6. Masoudi, A.; Belal, M.; Newson, T.P. A distributed optical fibre dynamic strain sensor based on phase-OTDR. *Meas. Sci. Technol.* **2013**, *24*, 085204. [CrossRef]
7. Fang, G.; Xu, T.; Feng, S.; Li, F. Phase-Sensitive Optical Time Domain Reflectometer Based on Phase-Generated Carrier Algorithm. *J. Light. Technol.* **2015**, *33*, 2811–2816. [CrossRef]
8. Pastor-Graells, J.; Martins, H.F.; Garcia-Ruiz, A.; Martin-Lopez, S.; Gonzalez-Herraez, M. Single-shot distributed temperature and strain tracking using direct detection phase-sensitive OTDR with chirped pulses. *Opt. Express* **2016**, *24*, 13121–13133. [CrossRef] [PubMed]

9. Masoudi, A.; Newson, T.P. High spatial resolution distributed optical fiber dynamic strain sensor with enhanced frequency and strain resolution. *Opt. Lett.* **2017**, *42*, 290–293. [CrossRef] [PubMed]
10. Wang, C.; Wang, C.; Shang, Y.; Liu, X.; Peng, G. Distributed acoustic mapping based on interferometry of phase optical time-domain reflectometry. *Opt. Commun.* **2015**, *346*, 172–177. [CrossRef]
11. Lu, Y.; Zhu, T.; Chen, L.; Bao, X. Distributed Vibration Sensor Based on Coherent Detection of Phase-OTDR. *J. Light. Technol.* **2010**, *28*, 3243–3249.
12. Pan, Z.; Liang, K.; Ye, Q.; Cai, H.; Qu, R.; Fang, Z. Phase-sensitive OTDR system based on digital coherent detection. *Proc. SPIE* **2011**, *8311*, 1–6.
13. Alekseev, A.E.; Vdovenko, V.S.; Gorshkov, B.G.; Potapov, V.T.; Simikin, D.E. A phase-sensitive optical time-domain reflectometer with dual-pulse diverse frequency probe signal. *Laser Phys.* **2015**, *25*, 065101. [CrossRef]
14. Wang, Z.; Pan, Z.; Fang, Z.; Ye, Q.; Lu, B.; Cai, H.; Qu, R. Ultra-broadband phase-sensitive optical time-domain reflectometry with a temporally sequenced multi-frequency source. *Opt Lett.* **2015**, *40*, 5192–5195. [CrossRef] [PubMed]
15. Wang, Z.; Zhang, L.; Wang, S.; Xue, N.; Peng, F.; Fan, M.; Sun, W.; Qian, X.; Rao, J.; Rao, Y. Coherent Φ-OTDR based on I/Q demodulation and homodyne detection. *Opt. Express* **2016**, *24*, 853–858. [CrossRef] [PubMed]
16. Lu, B.; Pan, Z.; Wang, Z.; Zheng, H.; Ye, Q.; Qu, R.; Cai, H. High spatial resolution phase-sensitive optical time domain reflectometer with a frequency-swept pulse. *Opt Lett.* **2017**, *42*, 391–394. [CrossRef] [PubMed]
17. Sun, Q.; Ai, F.; Liu, D.; Cheng, J.; Luo, H.; Peng, K.; Luo, Y.; Yan, Z.; Shum, P.P. M-OTDR sensing system based on 3D encoded microstructures. *Sci. Rep.* **2017**, *7*, 41137. [CrossRef] [PubMed]
18. Fan, Z.; Yixin, Z.; Lan, X.; Xuelin, W.; Xuping, Z. Improved Φ-OTDR Sensing System for High-Precision Dynamic Strain Measurement Based on Ultra-Weak Fiber Bragg Grating Array. *J. Light. Technol.* **2015**, *33*, 4775–4780. [CrossRef]
19. Wang, C.; Shang, Y.; Liu, X.-H.; Wang, C.; Yu, H.-H.; Jiang, D.-S.; Peng, G.-D. Distributed OTDR-interferometric sensing network with identical ultra-weak fiber Bragg gratings. *Opt. Express* **2015**, *23*, 29038–29046. [CrossRef] [PubMed]
20. Masoudi, A.; Newson, T.P. Contributed Review: Distributed optical fibre dynamic strain sensing. *Rev. Sci. Instrum.* **2016**, *87*, 011501. [CrossRef] [PubMed]
21. Muanenda, Y. Recent Advances in Distributed Acoustic Sensing Based on Phase-Sensitive Optical Time Domain Reflectometry. *J. Sens.* **2018**, *2018*, 16. [CrossRef]
22. He, H.; Shao, L.; Li, H.; Pan, W.; Luo, B.; Zou, X.; Yan, L. SNR Enhancement in Phase-Sensitive OTDR with Adaptive 2-D Bilateral Filtering Algorithm. *IEEE Photonics J.* **2017**, *9*, 1–10. [CrossRef]